

Chiral symmetry and its manifestation in optical responses in graphene: interaction and multi-layers

Y. Hatsugai

Institute of Physics, University of Tsukuba, Tsukuba 305-8571 Japan

E-mail: hatsugai.yasuhiro.ge@u.tsukuba.ac.jp

T. Morimoto

Condensed Matter Theory Laboratory, Riken, Saitama 351-0198, Japan

T. Kawarabayashi

Department of Physics, Toho University, Funabashi 274-8510, Japan

Y. Hamamoto

Institute of Physics, University of Tsukuba, Tsukuba 305-8571, Japan

H. Aoki

Department of Physics, University of Tokyo, Hongo, Tokyo 113-0033, Japan

Abstract. Chiral symmetry, fundamental in the physics of graphene, guarantees the existence of topologically stable doubled Dirac cones and anomalous behaviors of the zero-energy Landau level in magnetic fields. The crucial role is inherited in the optical responses and many-body physics in graphene, which are explained in this paper. We also give an overview of multilayer graphene from the viewpoint of the optical properties and their relation with the chiral symmetry.

1. Introduction

While the Dirac cone physics in graphene is forming a new branch in the condensed-matter physics, there is an increasing fascination with optical responses in graphene[1, 2, 3]. The present article focuses on how the physics of massless Dirac cone and the optical properties of graphene are related. There, we stress the factor that links the two is the chiral symmetry. So the purpose of this paper is, first, to discuss the meaning of the chiral symmetry in terms of fundamental ingredients in graphene including interaction and multi-layer systems as well as optical responses.

So let us start with the Dirac cone, which comes from the symmetry of graphene. The honeycomb lattice structure of this material has two atoms per unit cell, and if

we focus on the two π -bands arising from this, the system is effectively described by a traceless hermite Hamiltonian, $H(k) = R(k) \cdot \sigma$, which is parametrized by R with three real components. This implies that the Dirac cone has a co-dimension of three[4]. Since the momentum in two dimensions are described by two parameters, the Dirac cones do not arise in general, while the symmetry of the graphene at K and K' points gives rise to the Dirac cones. Here the key ingredient is the chiral symmetry of the honeycomb lattice. When the lattice points are classified into two sublattices and the hopping of electrons is only allowed between them, the system is chiral-symmetric. Then we can show that the degree of freedom in R is reduced from three to two. This also ensures the topological stability (against various modifications) of the Dirac cones of the chiral symmetric two-dimensional system, since the degeneracy cannot be removed by small but finite modifications as far as the chiral symmetry (or its extension) is respected.

A conspicuous feature is graphene and related models is that the Dirac cones appear in pairs (at K and K' points in graphene). This is due to the well-known fermion doubling in chiral-symmetric systems, which is a two-dimensional analogue of the Nielsen-Ninomiya theorem in four-dimensional lattice gauge theory[5, 6]. In a real graphene, the chiral symmetry is not rigorously valid. In the standard tight-binding parameters for graphene [7], however, most of the chiral-symmetry-breaking parameters are significantly smaller than the chiral symmetric ones in magnitude.

2. Chiral symmetry

Let us start with the chiral symmetry of fermions on a lattice, which is directly applicable to graphene. Assuming the lattice is bipartite, that is, all of the lattice points can be divided into two sublattice sites \bullet and \circ , the non-interacting Hamiltonian \mathcal{H}_0 is expressed as block-off diagonal form,

$$\mathcal{H}_0(D) = c^\dagger H_0 c = c^\dagger_\bullet D c_\circ + \text{h.c.}, \quad (1)$$

$$H_0 = \begin{bmatrix} O & D \\ D^\dagger & O \end{bmatrix}, \quad c = \begin{bmatrix} c_\bullet \\ c_\circ \end{bmatrix}, \quad c_\bullet = \begin{bmatrix} c_{1\bullet} \\ \vdots \\ c_{N_\bullet} \end{bmatrix}, \quad c_\circ = \begin{bmatrix} c_{1\circ} \\ \vdots \\ c_{N_\circ} \end{bmatrix} \quad (2)$$

where N_\bullet and N_\circ are the numbers of \bullet and \circ sites, respectively, and D is an $N_\bullet \times N_\circ$ matrix. We can introduce the chiral operator Γ that has

$$\{H_0, \Gamma\} = 0, \quad \Gamma = \begin{bmatrix} I_{N_\bullet} & O \\ O & -I_{N_\circ} \end{bmatrix} \quad (3)$$

where $\Gamma^2 = I_N$, $N = N_\bullet + N_\circ$ and $\text{Tr} \Gamma = N_\bullet - N_\circ$.

The chiral symmetry $\{H, \Gamma\} = 0$ implies that, if φ_i is an eigenstate of H with energy λ_i $\Gamma\varphi_i$ is another eigenstate with energy $-\lambda_i$ ($H_0\Gamma\varphi_i = -\Gamma H_0\varphi_i = -\lambda_i\Gamma\varphi_i$).

Without loss of generality, let us assume $N_\bullet \geq N_\circ$. Then the secular equation becomes

$$0 = \det_N(\lambda I_N - H_0) = \det_N \begin{bmatrix} \lambda I_{N_\bullet} & -D \\ -D^\dagger & \lambda I_{N_\circ} \end{bmatrix} = \det_N \begin{bmatrix} \lambda I_{N_\bullet} & -D \\ O & -\lambda^{-1} D^\dagger D + \lambda I_{N_\circ} \end{bmatrix} \quad (4)$$

$$= \lambda^{N_\bullet - N_\circ} \det_{N_\circ}(\lambda^2 I_{N_\circ} - D^\dagger D). \quad (5)$$

This implies, at least, $N_\bullet - N_\circ$ of the ϵ_j 's are zero. These zero energy states (zero modes) are geometrical since the number of these exact zero-energy states is determined by the geometrical structure of the lattice.

2.1. Chiral basis for the zero modes

As for a zero-energy state, its chiral partner is degenerated in energy. This implies that there is a gauge freedom in choosing the basis. In this paper, we focus on the zero-energy Landau level in graphene.

Before proceeding, we have to take care a bit about what we really mean by the zero-energy Landau level. Rigorously speaking, the $n = 0$ Landau level has the energy exactly equal to zero only for massless Dirac fermions in a continuous model. Conversely, if you consider a lattice model such as honeycomb tight-binding model, the $n = 0$ Landau level has in general a finite width, and the zero-energy condition is only realized in the limit of weak magnetic fields ($\phi \rightarrow 0$ where ϕ is the flux per hexagon). In a numerical calculation for the honeycomb lattice model with a finite ϕ , the $n = 0$ Landau level has a small but finite width. Still, we want to project the problem onto the $n = 0$ Landau level. For this purpose, we can define the ϵ -zero mode by collecting those states that have energies between $-\epsilon$ and ϵ , where $\epsilon(> 0)$ means the width of the Landau level. These naturally include the geometrical zero modes discussed above.

Now let us take an orthonormalized basis for the ϵ -zero modes which form an M -dimensional multiplet as $\psi = (\psi_1, \dots, \psi_M)$ ($\psi_i^\dagger \psi_j = \delta_{ij}$).

$$\langle \psi_i^\dagger | H_0^2 | \psi_i \rangle \leq \epsilon^2 \quad (6)$$

for $\forall i$. This property is inherited by a unitary-transformed $\psi_\omega = ((\psi_\omega)_1, \dots, (\psi_\omega)_M) = \psi_\omega$ for $\omega \in U(M)$. It implies the ϵ -zero modes are $U(M)$ gauge invariant.

Then one can construct a normalized complete multiplet as

$$\psi_T = (\psi, \varphi, \Gamma\varphi). \quad (7)$$

where φ is a multiplet of negative energy states $H_0\varphi_i = -\lambda_i\varphi$, $\lambda_i > \epsilon$ and $\Gamma\varphi$ is a multiplet of the chiral partners of φ . The normalization and the orthogonality of all the states are expressed as

$$\psi_T^\dagger \psi_T = \begin{bmatrix} \psi^\dagger \psi & \psi^\dagger \varphi & \psi^\dagger \Gamma\varphi \\ \varphi^\dagger \psi & \varphi^\dagger \varphi & \varphi^\dagger \Gamma\varphi \\ \varphi^\dagger \Gamma\psi & \varphi^\dagger \Gamma\varphi & \varphi^\dagger \varphi \end{bmatrix} = \begin{bmatrix} I_M & 0 & 0 \\ 0 & I_{M'} & 0 \\ 0 & 0 & I_{M'} \end{bmatrix} \quad (8)$$

where M' is the dimension of the negative (positive) energy multiplet φ ($\Gamma\varphi$). The completeness reads

$$\psi_T \psi_T^\dagger = \psi \psi^\dagger + \varphi \varphi^\dagger + \Gamma\varphi \varphi^\dagger \Gamma = I_N. \quad (9)$$

With this multiplet ψ_T , H_0 is block diagonalized as

$$H_0\psi_T = \psi_T \begin{bmatrix} \mathcal{E} & 0 & 0 \\ 0 & -\Lambda & 0 \\ 0 & 0 & \Lambda \end{bmatrix} \quad (10)$$

$$\mathcal{E} = \psi^\dagger H_0 \psi, \quad \bar{\mathcal{E}}^2 \equiv \text{Tr}\mathcal{E}^2/M \leq \epsilon^2, \quad \Lambda = \text{diag}(\lambda_1, \dots, \lambda_{M'}) \quad (\lambda_j > \epsilon). \quad (11)$$

Due to the completeness and orthogonality relations Eq.(8), we have

$$\Gamma\psi = \psi_T\psi_T^\dagger\Gamma\psi = \psi\psi^\dagger\Gamma\psi + \varphi\varphi^\dagger\Gamma\psi + \Gamma\varphi\varphi^\dagger\Gamma^2\psi = \psi\Gamma_0, \quad (12)$$

$$\Gamma_0 = \psi^\dagger\Gamma\psi, \quad (13)$$

where the $M \times M$ -dimensional hermitian matrix Γ_0 satisfies $\Gamma_0^2 = I_M$. Its trace is evaluated as

$$\text{Tr}\Gamma_0 = \text{Tr}\Gamma(\psi\psi^\dagger) = \text{Tr}\Gamma - 2\text{Tr}\Gamma(\varphi\varphi^\dagger) = \text{Tr}\Gamma = N_\bullet - N_\circ \quad (14)$$

Then Γ_0 is diagonalized as

$$\Gamma_0 = \omega_\Gamma \Gamma_{M_+M_-} \omega_\Gamma^\dagger, \quad (15)$$

$$\Gamma_{M_+M_-} = \begin{bmatrix} I_{M_+} & O \\ O & -I_{M_-} \end{bmatrix}, \quad M_+ - M_- = N_\bullet - N_\circ, \quad (16)$$

where $\omega_\Gamma \in U(M)$ with $M_+ + M_- = M$. Now let us define a chiral multiplet $\psi_\Gamma = \psi\omega_\Gamma$ that satisfies

$$\Gamma\psi_\Gamma = \psi_\Gamma\Gamma_{M_+M_-}, \quad \psi_\Gamma = (\psi_+, \psi_-), \quad (17)$$

$$\Gamma\psi_+ = \psi_+, \quad \psi_+ = (\psi_{1+}, \dots, \psi_{M_++}), \quad (18)$$

$$\Gamma\psi_- = -\psi_-. \quad \psi_- = (\psi_{1-}, \dots, \psi_{M--}). \quad (19)$$

Namely, $\psi_{i\pm}$'s are eigenstates of Γ as

$$\Gamma\psi_{i\pm} = \pm\psi_{i\pm}, \quad (20)$$

$$\psi_+ = \begin{bmatrix} \psi_\bullet \\ 0 \end{bmatrix}, \quad \psi_- = \begin{bmatrix} 0 \\ \psi_\circ \end{bmatrix}, \quad (21)$$

where ψ_\bullet is an $N_\bullet \times M_+$ matrix and ψ_\circ an $N_\circ \times M_-$ matrices.

3. Electron-electron interaction and chiral condensate in a magnetic field

Let us move on to discuss the electron-electron interaction in graphene in magnetic fields.

3.1. Two-body interactions

As for the electron-electron interaction, we take the two-body interaction $V_{ij}n_in_j$ between sites $\langle ij \rangle$, which can include long-range interactions. Note that

$$n_in_j = c_i^\dagger c_i c_j^\dagger c_j = c_i^\dagger c_j^\dagger c_j c_i = -1 + n_i + n_j + c_i c_j c_j^\dagger c_i^\dagger. \quad (22)$$

We can express the interaction in an electron-hole symmetric form, at half-filling, as

$$\mathcal{H}_{int} = \sum_{ij} V_{ij} \left(n_i - \frac{1}{2} \right) \left(n_j - \frac{1}{2} \right) = \frac{1}{2} \sum_{\langle ij \rangle} V_{ij} \left[c_i^\dagger c_j^\dagger c_j c_i + (c \rightleftharpoons c^\dagger) \right] + \text{const.} \quad (23)$$

3.2. Ground state within the projected subspace

We assume that the electron-electron interaction is sufficiently weak as compared with the Landau gap between the $n = 0$ Landau level and those for $n = \pm 1$. When the filling factor of the $n = 0$ LL is $\nu < 1$, the ground state is then given by the configurations of the $n = 0$ LL states, while the filled states below them can be regarded as the ‘‘Dirac sea’’. The one-particle spectrum in graphene is given by the ϵ -zero modes and the chiral pairs of non-zero energy states as discussed above. Then the kinetic energy from the ϵ -zero modes is negligible, so that the ground state is given perturbatively (i.e., in the interaction energy that is smaller than the Landau gap) as

$$|\Psi\rangle = \sum_{i_1, \dots, i_M \subset \{1, \dots, M\}} C_{i_1, \dots, i_M} d_{i_1}^\dagger \cdots d_{i_M}^\dagger |D_{<}\rangle, \quad |D_{<}\rangle = \prod_{j=1}^{M'} d_{<j}^\dagger |0\rangle, \quad (24)$$

where $|D_{<}\rangle$ is the filled Dirac sea ($d_i |D_{<}\rangle = 0$ for all i 's), $\{i_1, \dots, i_M\}$ a subset of the ϵ -zero modes, and M the number of particles. The free-fermion Hamiltonian \mathcal{H}_0 (i.e., the kinetic energy) is written as

$$\mathcal{H}_0 = c^\dagger \psi_T \text{diag}(\mathcal{E}, -\Lambda, \Lambda) \psi_T^\dagger c = d^\dagger \mathcal{E} d - d_{<}^\dagger \Lambda d_{<} + d_{>}^\dagger \Lambda d_{>}, \quad (25)$$

$$\begin{bmatrix} d \\ d_{<} \\ d_{>} \end{bmatrix} = \psi_T^\dagger c = \begin{bmatrix} \psi^\dagger c \\ \varphi^\dagger c \\ \varphi^\dagger \Gamma c \end{bmatrix}, \quad c = \psi_T \begin{bmatrix} d \\ d_{<} \\ d_{>} \end{bmatrix} = (\psi, \varphi, \Gamma \varphi) \begin{bmatrix} d \\ d_{<} \\ d_{>} \end{bmatrix} \quad (26)$$

where $d^\dagger = (d_1^\dagger, \dots, d_M^\dagger)$, $d_{<}^\dagger = (d_{<1}^\dagger, \dots, d_{<M'}^\dagger)$, and $d_{>}^\dagger = (d_{>1}^\dagger, \dots, d_{>M'}^\dagger)$ are standard fermion creation operators for the ϵ -zero mode, the negative energies and positive ones as $\{d_\ell, d_{\ell'}^\dagger\} = \delta_{\ell\ell'}$, $\{d_{<\ell}, d_{<\ell'}^\dagger\} = \delta_{\ell\ell'}$, $\{d_{>\ell}, d_{>\ell'}^\dagger\} = \delta_{\ell\ell'}$, etc.

3.3. Projected interaction and its symmetry

Now let us take the chiral basis for the ϵ -zero modes to describe the interaction between the particles. We assume that the perturbative ground state within the configuration of the $n = 0$ Landau level is determined by the projected interaction $\tilde{\mathcal{H}}_{int}$. The projected Hamiltonian is defined as

$$\tilde{\mathcal{H}}_{int} = \frac{1}{2} \sum_{ij} V_{ij} [\tilde{c}_i^\dagger \tilde{c}_j^\dagger \tilde{c}_j \tilde{c}_i + (c \rightleftharpoons c^\dagger)] = \frac{1}{2} \sum_{ij} V_{ij} (d^\dagger \psi^\dagger)_i (d^\dagger \psi^\dagger)_j (\psi d)_j (\psi d)_i + C.c., \quad (27)$$

where $C.c.$ is a charge conjugation defined below and \tilde{c}_i is a projected fermion defined as

$$\tilde{c} \equiv \Psi_T \begin{bmatrix} d \\ 0 \\ 0 \end{bmatrix} = (\psi, \varphi, \Gamma \varphi) \begin{bmatrix} d \\ 0 \\ 0 \end{bmatrix} = \psi d = \psi \psi^\dagger c = P c, \quad (28)$$

with $P = \psi\psi^\dagger = P^\dagger$ being the projection to the ϵ -zero modes. These \tilde{c}_i 's are not canonical fermions, since

$$\{\tilde{c}_i, \tilde{c}_j^\dagger\} = \{(P)_{ii'}c_{i'}, c_{j'}^\dagger(P^\dagger)_{j'j}\} = (PP^\dagger)_{ij} = (P^2)_{ij} = (P)_{ij}. \quad (29)$$

Note that the projected Hamiltonian is clearly positive semi-definite.

3.4. Chiral transformation and charge conjugation

Let us take a chiral basis to define canonical fermions d_i for the ϵ -zero modes, defined as

$$d = \begin{bmatrix} d_+ \\ d_- \end{bmatrix} = \psi_\Gamma^\dagger c = \begin{bmatrix} \psi_\bullet^\dagger & O \\ O & \psi_\circ^\dagger \end{bmatrix} c = \begin{bmatrix} \psi_\bullet^\dagger c_\bullet \\ \psi_\circ^\dagger c_\circ \end{bmatrix} \quad (30)$$

$$d_+ = \begin{bmatrix} d_{1+} \\ \vdots \\ d_{M_{++}} \end{bmatrix}, \quad d_- = \begin{bmatrix} d_{1-} \\ \vdots \\ d_{M_{--}} \end{bmatrix} \quad (31)$$

$$\tilde{c} = \begin{bmatrix} \tilde{c}_\bullet \\ \tilde{c}_\circ \end{bmatrix} = \begin{bmatrix} \psi_\bullet & 0 \\ 0 & \psi_\circ \end{bmatrix} d = \begin{bmatrix} \psi_\bullet d_+ \\ \psi_\circ d_- \end{bmatrix} \quad (32)$$

We can define a chiral transformation \mathcal{U}_θ as

$$\mathcal{O} \mapsto \mathcal{U}_\theta^\dagger \mathcal{O} \mathcal{U}_\theta, \quad \mathcal{U}_\theta = e^{i\theta\mathcal{G}}, \quad (33)$$

where the generator of the transformation, the chirality \mathcal{G} , is given as

$$\mathcal{G} = \tilde{c}^\dagger \Gamma \tilde{c} = \sum_{i \in \bullet} \tilde{c}_i^\dagger \tilde{c}_i - \sum_{i \in \circ} \tilde{c}_i^\dagger \tilde{c}_i = d^\dagger \psi_\Gamma^\dagger \Gamma \psi_\Gamma d = d^\dagger \Gamma_0 d = d_+^\dagger d_+ - d_-^\dagger d_-. \quad (34)$$

The chiral transformation operates as

$$d \mapsto d_\theta = \mathcal{U}_\theta^\dagger d \mathcal{U}_\theta = e^{i\theta\mathcal{G}} d e^{-i\theta\mathcal{G}} = e^{-i\theta\Gamma_0} d = \begin{bmatrix} e^{-i\theta} d_+ \\ e^{i\theta} d_- \end{bmatrix} \quad (35)$$

$$\tilde{c}_i \mapsto \begin{cases} e^{-i\theta} \tilde{c}_i & i \in \bullet \\ e^{+i\theta} \tilde{c}_i & i \in \circ \end{cases} \quad (36)$$

Then it is clear that the projected interaction is invariant under the chiral transformation as

$$\tilde{\mathcal{H}}_{int} \mapsto e^{-i\theta\mathcal{G}} \tilde{\mathcal{H}}_{int} e^{+i\theta\mathcal{G}} = \tilde{\mathcal{H}}_{int}. \quad (37)$$

For an infinitesimal transformation this implies a conservation law,

$$[\mathcal{G}, \tilde{\mathcal{H}}_{int}] = 0. \quad (38)$$

Let us next define a charge conjugation which is anti-unitary as

$$\mathcal{O} \mapsto \mathcal{A}_C^\dagger \mathcal{O} \mathcal{A}_C, \quad (39)$$

$$\mathcal{A}_C = K \prod_{\ell=1}^M (d_\ell + d_\ell^\dagger) \prod_{\ell=1}^{M'} (d_{<\ell} + d_{<\ell}^\dagger) (d_{>\ell} + d_{>\ell}^\dagger), \quad (40)$$

where K is complex-conjugation with $K^2 = 1$. Its operation is, for example,

$$\mathcal{A}_C^\dagger d_\ell \mathcal{A}_C = (-)^{N-1} d_\ell^\dagger, \quad \mathcal{A}_C^\dagger d_\ell^\dagger \mathcal{A}_C = (-)^{N-1} d_\ell. \quad (41)$$

Then the invariance of the interaction Hamiltonian under the charge conjugation,

$$\mathcal{A}_C^\dagger \tilde{\mathcal{H}}_{int} \mathcal{A}_C = \tilde{\mathcal{H}}_{int} \quad (42)$$

trivially follows.

3.5. Chiral condensate as doubly-degenerate ground states

In this section, we restrict ourselves to consider a repulsive interaction that only acts between \bullet and \circ sites. The projected interaction in this case is written as

$$\begin{aligned} \tilde{\mathcal{H}}_{int} &= \frac{1}{2} \sum_{i \bullet j \circ} V_{i \bullet j \circ} (\tilde{c}_{i \bullet}^\dagger \tilde{c}_{j \circ}^\dagger \tilde{c}_{j \circ} \tilde{c}_{i \bullet} + C.c) \quad (43) \\ &= \frac{1}{2} \sum_{i \bullet j \circ} V_{i \bullet j \circ} \left[(d_+^\dagger \psi_\bullet^\dagger)_i (d_-^\dagger \psi_\circ^\dagger)_j (\psi_\circ d_-)_j (\psi_\bullet d_+)_i + (\psi_\bullet d_+)_i (\psi_\circ d_-)_j (d_-^\dagger \psi_\circ^\dagger)_j (d_+^\dagger \psi_\bullet^\dagger)_i \right] \quad (44) \end{aligned}$$

where $\exists V_{i \bullet j \circ} > 0$. Here we allow any repulsive interaction between the \bullet and \circ sites.

Now we can readily see that the two states,

$$\tilde{\mathcal{H}}_{int} |G_\pm\rangle = 0, \quad |G_\pm\rangle = d_{1\pm}^\dagger \cdots d_{M_\pm}^\dagger |D_\pm\rangle, \quad (45)$$

which have maximum and minimum chiralities, respectively, are special, since each of them has vanishing interaction energy. As for $|G_+\rangle$, for example, all $d_{\ell+}$ states are filled, $(d_+^\dagger \psi_\bullet^\dagger)_i |G_+\rangle = 0$. Also none of the $d_{\ell-}$ states are occupied, $(\psi_\circ d_-)_j |G_+\rangle = 0$. Since the interaction Hamiltonian $\tilde{\mathcal{H}}_{int}$ is semi-positive definite, these two states are ground states of $\tilde{\mathcal{H}}_{int}$ with a degeneracy of two.

As for the chiral transformation, we have

$$|G_\pm\rangle \mapsto \mathcal{U}_\theta^\dagger |G_\pm\rangle = e^{\mp i M_\pm \theta} |G_\pm\rangle, \quad (46)$$

where \mathcal{U}_χ is the chiral operation defined above. This property follows, since $|G_\pm\rangle$ are eigenstates of the chirality \mathcal{G} as

$$\mathcal{G} |G_\pm\rangle = \pm M_\pm |G_\pm\rangle. \quad (47)$$

Thus we have shown that the ground states are the *chiral condensates*, where the chirality is macroscopic ($M_\pm \sim N$).

As for the charge conjugation, it operates as

$$|G_\pm\rangle \mapsto (-)^S d_{1\mp}^\dagger \cdots d_{M_\mp}^\dagger |D_\mp\rangle, \quad (48)$$

where the $|D_\mp\rangle$ is the positive Dirac sea up to the sign.

3.6. Chiral-condensate doublet as a Hall insulator

The Hall conductance of the doubly-degenerate chiral condensates can be calculated with the Niu-Thouless-Wu formula as

$$\sigma_{xy} = \frac{e^2}{h} \frac{1}{N_D} C, \quad C = \frac{1}{2\pi i} \int \text{Tr}_2 F, \quad F = dA + A^2, \quad A = \Psi^\dagger d\Psi, \quad (49)$$

where $\Psi = (|G_+\rangle, |G_-\rangle)$ is the chiral-condensed ground states with the degeneracy of $N_D = 2$.

The doublet, being degenerate, can be mixed, but diagonalization of the chirality \mathcal{G} acts to fix the gauge. Here we assume a finite energy gap above the ground state multiplet. Then the Chern number of the doublet becomes well-defined, and given by the sum of each as

$$C = C_+ + C_-, \quad (50)$$

where C_\pm is the Chern number for $|G_\pm\rangle$. Further, we can decompose the condensate as

$$C_\pm = C_{\psi_\pm} + C_{D_\pm}, \quad (51)$$

$$C_{\psi_\pm} = \frac{1}{2\pi i} \int \text{Tr}_{M_\pm} d\psi_\pm^\dagger d\psi_\pm, \quad C_{D_\pm} = \frac{1}{2\pi i} \int \langle dD_\pm | dD_\pm \rangle, \quad (52)$$

where C_{D_\pm} is the Chern number of the filled Dirac sea. Since the chiral operator Γ is unitary, the Chern number of the positive Dirac sea is the same as that of the negative Dirac sea as

$$C_{D_>} = \frac{1}{2\pi i} \int \langle dD_> | dD_> \rangle = C_{D_<} \equiv C_D. \quad (53)$$

Since the charge conjugation is anti-unitary, it implies

$$C_{D_>} + C_{\psi_-} = -(C_{D_<} + C_{\psi_+}), \quad (54)$$

which in turn gives the total Chern number of the doubly degenerate chiral condensate as

$$C = (C_{D_<} + C_{\psi_-}) + (C_{D_<} + C_{\psi_+}) = C_{\psi_-} + C_{\psi_+} + 2C_D = 0. \quad (55)$$

This implies that the half-filled state formed by the chiral doublet is a *Hall insulator* with the topological degeneracy of 2.

4. Multilayer graphene and chiral symmetry

4.1. Bilayer/trilayer Hamiltonians

Let us start with the bilayer graphene in magnetic fields[6]. With $j = (j_1, j_2)$ denoting two-dimensional coordinates, $e_{1,2}$ the unit translations, and φ the total flux per hexagon in units of the flux quantum $\varphi_0 = h/e$ (see Fig.1), the Hamiltonian is written as

$$\mathcal{H}^{\text{bilayer}} = H_d + H_u + H_{ud}, \quad (56)$$

$$\begin{aligned} \mathcal{H}_d = \gamma_0 \sum_j \left[d_\bullet^\dagger(j) d_\circ(j) \right. \\ \left. + e^{i2\pi\varphi j_1} d_\bullet^\dagger(j) d_\circ(j - e_2) + e^{-i2\pi\varphi(j_1 + \frac{3}{6})} d_\bullet^\dagger(j + e_1) d_\circ(j) + \text{h.c.} \right], \end{aligned} \quad (57)$$

$$\mathcal{H}_u = \mathcal{H}_d(d \rightarrow u, j_1 \rightarrow j_1 + 2/6) \quad (58)$$

$$\begin{aligned} \mathcal{H}_{ud} = \sum_j \left[\gamma_1 u_\bullet^\dagger(j) d_\circ(j) \right. \\ \left. + \gamma_3 \left(e^{i2\pi\varphi(j_1 + \frac{1}{6})} d_\bullet^\dagger(j) + d_\bullet^\dagger(j + e_1) + e^{-i2\pi\varphi(j_1 + \frac{4}{6})} d_\bullet^\dagger(j + e_1 - e_2) \right) u_\circ(j - e_2) + \text{h.c.} \right] \end{aligned} \quad (59)$$

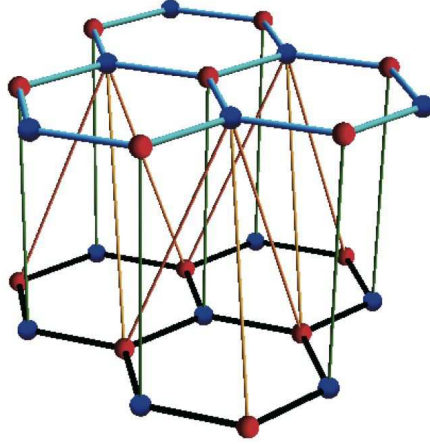


Figure 1. Lattice structure of the bilayer graphene. Interlayer couplings γ_1 and γ_3 are denoted by green and yellow bonds, respectively.

Here "u(d)" denote up (down) layers, γ_0 is the nearest-neighbor hopping within each layer, and γ_1 the inter-layer hopping perpendicular to the layer. The hopping γ_3 , the second largest inter-layer hopping, is along an oblique direction, causes trigonal deformation of the energy dispersion (trigonal warping)[8] in zero magnetic field. In a finite magnetic field, the hopping acquires Peierls phases appearing in the Hamiltonian above, again due to the oblique directions of the hopping.

As for the trilayer, we have

$$\mathcal{H}^{\text{trilayer}} = \mathcal{H}_d + \mathcal{H}_u + \mathcal{H}_t + \mathcal{H}_{ud} + \mathcal{H}_{ut}^{ABA,ABC} \quad (60)$$

$$\mathcal{H}_t = \mathcal{H}_d(d \rightarrow t, j_1 \rightarrow j_1 + 4/6) \quad (61)$$

$$H_{ut}^{ABC} = \mathcal{H}_{ud}(d \rightarrow u, u \rightarrow t, j_1 \rightarrow j_1 + 2/6) \quad (62)$$

$$H_{ut}^{ABA} : H_{ud}(d \rightarrow t, u \rightarrow u). \quad (63)$$

Here we have added "t" (top layer) on top of the "d, u" (down, up) layers, and ABA (ABC) stand for the trilayer graphene with the ABA (ABC) stacking.

Now let us Fourier-transform the fermion operators, first along the e_2 direction as

$$d_\alpha, u_\alpha, t_\alpha(j) = \int_{-\pi}^{\pi} \frac{dk_2}{2\pi} e^{ik_2 j_2} d_\alpha, u_\alpha, t_\alpha(j_1, k_2). \quad (64)$$

Then we have

$$\mathcal{H}^b = \int_{-\pi}^{\pi} \frac{dk_2}{2\pi} \mathcal{H}^{1D,b}(k_2), \quad \mathcal{H}^t = \int_{-\pi}^{\pi} \frac{dk_2}{2\pi} \mathcal{H}^{1D,t}(k_2), \quad (65)$$

$$\mathcal{H}^{1D,b}(k_2) = \mathcal{H}_d^{1D}(k_2) + \mathcal{H}_u^{1D}(k_2) + \mathcal{H}_{du}^{1D}(k_2), \quad (66)$$

$$\mathcal{H}^{1D,t}(k_2) = \mathcal{H}_d^{1D}(k_2) + \mathcal{H}_u^{1D}(k_2) + \mathcal{H}_t^{1D}(k_2) + \mathcal{H}_{du}^{1D}(k_2) + \mathcal{H}_{ut}^{1D,ABC(ABA)}(k_2), \quad (67)$$

$$\begin{aligned} \mathcal{H}_d^{1D}(k_2) = \gamma_0 \sum_{j_1} \left[(1 + e^{i(2\pi\varphi j_1 - k_2)}) d_{\bullet}^{\dagger}(j_1, k_2) d_{\circ}(j_1, k_2) \right. \\ \left. + e^{-i2\pi\varphi(j_1 + \frac{3}{6})} d_{\bullet}^{\dagger}(j_1 + 1, k_2) d_{\circ}(j_1, k_2) + \text{h.c.} \right], \end{aligned} \quad (68)$$

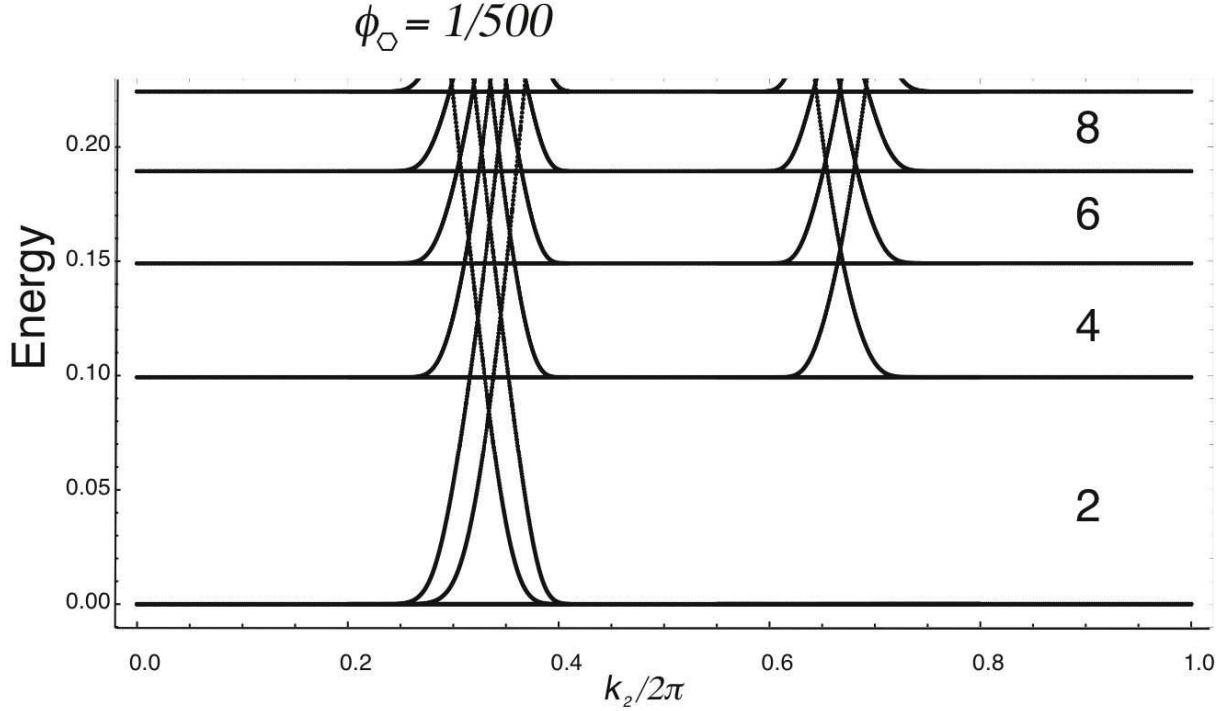


Figure 2. Energy spectrum in the region around the $n = 0$ Landau level in the bilayer graphene with zigzag edges and a periodic boundaries orthogonal to those (along e_2). Here we have a relatively small magnetic field $\phi = 1/500$, with $\gamma_0 = 1.0$ and $\gamma_1 = 0.2$. The attached numbers denote the Hall conductivity when E_F is in each interval between the Landau levels, which coincide with the number of edge modes (curves traversing different Landau levels).

$$\mathcal{H}_u^{1D}(k_2) = \mathcal{H}_d^{1D}(k_2) : d \rightarrow u, j_1 \rightarrow j_1 + 2/6, \quad (69)$$

$$\mathcal{H}_t^{1D}(k_2) = \mathcal{H}_d^{1D}(k_2) : d \rightarrow t, j_1 \rightarrow j_1 + 4/6, \quad (70)$$

$$\mathcal{H}_{du}^{1D}(k_2) = \sum_{j_1} \left[\gamma_1 u_{\bullet}^{\dagger}(j_1, k_2) d_{\circ}(j_1, k_2) + \gamma_3 \left(e^{i(-k_2 + 2\pi\phi(j_1 + \frac{1}{6}))} d_{\bullet}^{\dagger}(j_1, k_2) + (e^{-k_2} + e^{-i2\pi\phi(j_1 + \frac{4}{6})}) d_{\bullet}^{\dagger}(j_1 + 1, k_2) \right) u_{\circ}(j_1, k_2) + \text{h.c.} \right] \quad (71)$$

$$\mathcal{H}_{ut}^{1D,ABC}(k_2) = \mathcal{H}_{du}^{1D}(k_2) : d \rightarrow u, u \rightarrow t, j_1 \rightarrow j_1 + 2/6, \quad (72)$$

$$\mathcal{H}_{ut}^{1D,ABA}(k_2) = \mathcal{H}_{du}^{1D}(k_2) : d \rightarrow t, u \rightarrow u. \quad (73)$$

In Fig.2, we have shown the spectrum of the bilayer graphene on a cylinder. Here the translational symmetry along e_2 makes the wave number k_2 a good quantum number, so that the dispersion against k_2 is depicted. The “bulk-edge correspondence”, which dictates bulk topological features such as the quantized Hall conductivity has a one-to-one correspondence to edge properties, allows us to obtain the Hall conductivity of the system by counting the number of edge modes.

4.2. Zero magnetic field

For zero magnetic field, we can make a Fourier transform along the e_1 as

$$u_\alpha, d_\alpha, t_\alpha(k_1, k_2) = \int_{-\pi}^{\pi} \frac{dk_1}{2\pi} e^{ik_1 j_1} u_\alpha, d_\alpha, t_\alpha(j_1, k_2), \quad (74)$$

we have a fully Fourier-transformed Hamiltonian. For the bilayer we have

$$\mathcal{H}^{\text{bilayer}} = \int \frac{d^2 k}{(2\pi)^2} \mathcal{H}(k) \quad (75)$$

$$\begin{aligned} \mathcal{H}(k) &= \gamma_0(1 + e^{-ik_2} + e^{-ik_1})(d_\bullet^\dagger d_\circ + u_\bullet^\dagger u_\circ) \\ &\quad + \gamma_1 u_\bullet^\dagger d_\circ + \gamma_3(e^{-ik_1} + e^{-ik_2} + e^{-i(k_1+k_2)})d_\bullet^\dagger u_\circ + \text{h.c.} \end{aligned} \quad (76)$$

$$= (u_\bullet^\dagger, d_\bullet^\dagger, u_\circ^\dagger, d_\circ^\dagger) H_b^L \begin{bmatrix} u_\bullet \\ d_\bullet \\ u_\circ \\ d_\circ \end{bmatrix} \quad (77)$$

$$H_b^L = \begin{bmatrix} O & D \\ D^\dagger & O \end{bmatrix}, \quad D = \begin{bmatrix} \Delta & \gamma_1 \\ \gamma'_3 & \Delta \end{bmatrix} \quad (78)$$

where

$$\Delta(k) = \gamma_0(1 + e^{-ik_1} + e^{-ik_2}), \quad (79)$$

$$\gamma'_3 = \gamma_3(e^{-ik_1} + e^{-ik_2} + e^{-ik_1}e^{-ik_2}). \quad (80)$$

For the trilayer, we have

$$\mathcal{H}^{\text{trilayer}} = \int \frac{d^2 k}{(2\pi)^2} \mathcal{H}(k), \quad (81)$$

$$\mathcal{H}(k) = \gamma_0(1 + e^{-ik_2} + e^{-ik_1})(d_\bullet^\dagger d_\circ + u_\bullet^\dagger u_\circ + t_\bullet^\dagger t_\circ) + \quad (82)$$

$$\text{(for ABC)} \quad + \gamma_1(t_\bullet^\dagger u_\circ + u_\bullet^\dagger d_\circ) + \gamma'_3(u_\bullet^\dagger t_\circ + d_\bullet^\dagger u_\circ) + \text{h.c.} \quad (83)$$

$$\text{(for ABA)} \quad + \gamma_1(u_\bullet^\dagger t_\circ + u_\bullet^\dagger d_\circ) + \gamma'_3(t_\bullet^\dagger u_\circ + d_\bullet^\dagger u_\circ) + \text{h.c.} \quad (84)$$

$$= (t_\bullet^\dagger, u_\bullet^\dagger, d_\bullet^\dagger, t_\circ^\dagger, u_\circ^\dagger, d_\circ^\dagger) H_t^L \begin{bmatrix} t_\bullet \\ u_\bullet \\ d_\bullet \\ t_\circ \\ u_\circ \\ d_\circ \end{bmatrix} \quad (85)$$

$$H_t^L = \begin{bmatrix} O & D^{ABC, ABA} \\ D^{ABC, ABA^\dagger} & O \end{bmatrix}, \quad (86)$$

$$D^{ABC} = \begin{bmatrix} \Delta & \gamma_1 & 0 \\ \gamma'_3 & \Delta & \gamma_1 \\ 0 & \gamma'_3 & \Delta \end{bmatrix}, \quad D^{ABA} = \begin{bmatrix} \Delta & \gamma'_3 & 0 \\ \gamma_1 & \Delta & \gamma_1 \\ 0 & \gamma'_3 & \Delta \end{bmatrix} \quad (87)$$

Further, we can extend the above argument to consider the ABC stacked graphene with a general number (p) of layers. In the present representation the Hamiltonian

simplifies into

$$H_p = \begin{bmatrix} O & D_p \\ D_p^\dagger & O \end{bmatrix}, \quad D_p = \Delta \mathbf{1} + \gamma_1 J_p + \gamma_3' \tilde{J}_p, \quad (88)$$

where $\mathbf{1}$ is a p -dimensional unit matrix and $J_p = \begin{bmatrix} 0 & 1 & 0 \\ 0 & 0 & \ddots \\ \vdots & \ddots & \ddots \end{bmatrix}$.

4.2.1. Low-energy Hamiltonians around K and K' The Dirac points (K and K' points) for the monolayer graphene are specified by $e^{-ik_1} = \omega$ and $e^{-ik_2} = \omega^2$, $\omega^3 = 1, \omega \neq 1$, at which Δ vanishes along with $\gamma_3' \rightarrow 0$. Around the Dirac points we can expand them as

$$\Delta = -i\gamma_0\omega\xi, \quad \gamma_3' = i\gamma_3\omega^2\xi^*, \quad \xi = \delta k_1 + \omega\delta k_2, \quad (89)$$

As for the multilayer graphene, gapless momenta are determined by $\det D$'s. For the bilayer, it is given as

$$\det D^{AB} = \Delta^2 - \gamma_1\gamma_3' = -\gamma_0^2\omega^2 \left(\xi^2 - \frac{i\gamma_1\gamma_3}{\gamma_0^2}\xi^* \right). \quad (90)$$

This vanishes at four points, $\xi = 0, \xi_0, \omega\xi_0, \omega^2\xi_0$, where $\xi_0 = (\gamma_1\gamma_3/\gamma_0^2)e^{i\pi/6}$. Namely, each Dirac point proliferates into four.

For the trilayer, it is

$$\det D^{ABC} = \det D^{ABA} = \Delta^3 - 2\Delta\gamma_1\gamma_3'. \quad (91)$$

This gives Dirac cones at $\xi = \sqrt{2}\xi_0, \sqrt{2}\xi_0\omega, \sqrt{2}\xi_0\omega^2$ and double zero at $\xi = 0$. One may discuss the case of p -layers as well.

The Dirac points in the chiral-symmetric system at $E = 0$ are specified by $\det D = 0$, for which the low-energy dispersion is given by $\epsilon(k) \propto \pm|\det D|$. In Fig.3, we have shown the low-energy dispersion along with $|\det D|$ and $\arg \det D$ for a finite value of γ_3 in the bilayer system. From this plot we can see that the chiralities of the four Dirac points are +1, -1, -1, -1 or -1, 1, 1, 1.

Now let us discuss the low-energy Hamiltonian in the absence of the trigonal warping ($\gamma_3 = 0$). If we denote the number of layers by p in the ABC-stacked p -layered graphene (including bilayer), D_p is triangular

$$D_p(k) = \gamma_1 \begin{bmatrix} z(k) & 1 & 0 \\ 0 & z(k) & 1 & \ddots \\ & \ddots & \ddots & \ddots \end{bmatrix}, \quad z(k) = \Delta(k)/\gamma_1, \quad (92)$$

$$\det D_p(k) = \Delta^p, \quad (93)$$

where taking a continuous limit around K and K' points implies we are assuming $|z| \ll 1$. Precisely at the K and K' points, we have $D_p^\dagger D_p = \gamma_1^2 \text{diag}(0, 1, 1, \dots)$, i.e., there exists only one low-energy mode for $D_p^\dagger D_p$ while the others have γ_1^2 . Then the chiral symmetry (i.e., H_p is composed of D_p as the off-diagonal block) implies that H_p has two low-energy

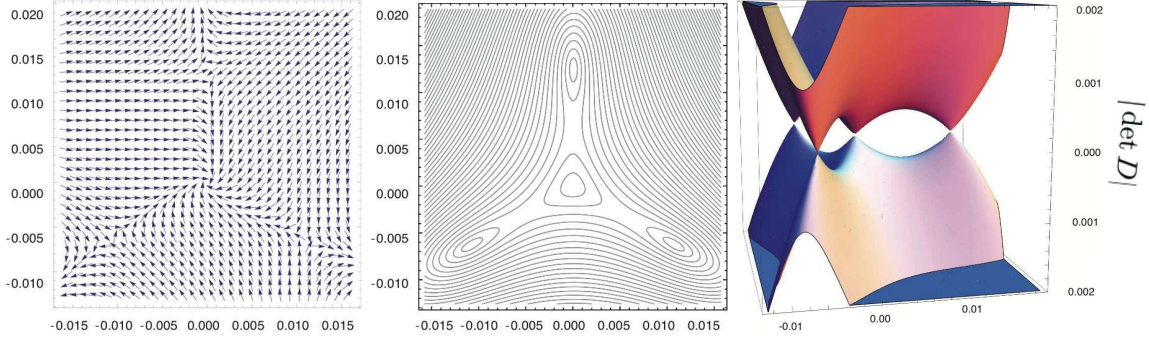


Figure 3. For the bilayer graphene in the presence of the trigonal warping ($\gamma_3 \neq 0$), we show $\text{Arg det } D$ (left panel), contours for $|\det D|$ (center), and $\det D$ (\propto the band dispersion; right). Here we take $\gamma_0 = 3.1$, $\gamma_1 = 0.4$, $\gamma_3 = 0.3$.

modes, $\pm\epsilon(k)$, with $\epsilon(k) = |\det D_p(k)|/\gamma_1^{p-1} = \gamma_1|z(k)|^p$. Here we can take the chiral basis introduced in previous sections to expand the low-energy doublet as

$$\psi = (\psi_+, \psi_-) = \begin{bmatrix} \psi_\bullet & 0 \\ 0 & \psi_\circ \end{bmatrix}, \quad D_p D_p^\dagger \psi_\bullet = \epsilon^2 \psi_\bullet, \quad D_p^\dagger D_p \psi_\circ = \epsilon^2 \psi_\circ \quad (94)$$

$\psi_{\bullet,\circ}$ are asymptotically normalized and ($|z| \ll 1$) given as

$$\psi_\bullet = \begin{bmatrix} (-z^*)^{p-1} \\ \vdots \\ -z^* \\ 1 \end{bmatrix}, \quad \psi_\circ = \begin{bmatrix} 1 \\ -z \\ \vdots \\ (-z)^{p-1} \end{bmatrix} \quad (95)$$

with $\psi_\bullet^\dagger \psi_\bullet = \psi_\circ^\dagger \psi_\circ = (1-|z|^p)(1-|z|^2)^{-1} = 1 + \mathcal{O}(|z|^2)$. They are consistent with Eq.(94) up to the errors arising from the normalization of $\psi_\bullet^\dagger \psi_\bullet$ and $\psi_\circ^\dagger \psi_\circ$. Then projecting out the high energy sectors, we have an effective Hamiltonian for the low-energy doublet formed by the chiral basis ψ (including the monolayer case) as

$$H_p^{\text{eff}} = \psi^\dagger H_p \psi = -\gamma_1 \begin{bmatrix} 0 & (-z)^p \\ (-z^*)^p & 0 \end{bmatrix} = (-\gamma_1)^{-(p-1)} \begin{bmatrix} 0 & \Delta^p \\ \Delta^{*p} & 0 \end{bmatrix} \quad (96)$$

As for the ABA trilayer, $(D^{ABA})^\dagger (D^{ABA})$ has two low-energy modes around the K and K' points, which implies the low-energy modes of H_3^{ABA} is spanned by a 4-dimensional orthonormalized chiral basis as

$$\psi = (\psi_+, \psi_-) = \begin{bmatrix} \psi_\bullet & 0 \\ 0 & \psi_\circ \end{bmatrix} = \begin{bmatrix} \psi_\bullet^{(1)} & \psi_\bullet^{(2)} & 0 & 0 \\ 0 & 0 & \psi_\circ^{(1)} & \psi_\circ^{(2)} \end{bmatrix}, \quad (97)$$

$$\psi^\dagger \psi = \text{diag}(1, 1, 1, 1) + \mathcal{O}(|z|), \quad (98)$$

$$D_p D_p^\dagger \psi_\bullet^{(i)} = \epsilon_i^2 \psi_\bullet^{(i)}, \quad D_p^\dagger D_p \psi_\circ^{(i)} = \epsilon_i^2 \psi_\circ^{(i)}, \quad \epsilon_1 = |\Delta|, \quad \epsilon_2 = \gamma_1^{-1} |\Delta|^2 / \sqrt{2}, \quad (99)$$

where we have, up to the leading order,

$$\psi_\bullet^{(1)} = \frac{1}{\sqrt{2}} \begin{bmatrix} -1 \\ 0 \\ 1 \end{bmatrix}, \quad \psi_\bullet^{(2)} = \frac{1}{\sqrt{2}} \begin{bmatrix} 1 \\ -z^* \\ 1 \end{bmatrix},$$

$$\psi_{\circ}^{(1)} = \frac{1}{\sqrt{2}} \begin{bmatrix} -1 \\ 0 \\ 1 \end{bmatrix}, \quad \psi_{\circ}^{(2)} = \frac{1}{2} \begin{bmatrix} -z \\ 2 \\ -z \end{bmatrix}. \quad (100)$$

Now we have $\psi^\dagger H_3^{ABA} \psi = \begin{bmatrix} O & \psi_{\bullet}^\dagger D \psi_{\circ} \\ \psi_{\circ}^\dagger D^\dagger \psi_{\bullet} & O \end{bmatrix}$ and $\psi_{\bullet}^\dagger D \psi_{\circ} = \gamma_1 \begin{bmatrix} z & 0 \\ 0 & -z^2/\sqrt{2} \end{bmatrix}$, we end up with a simple decomposition,

$$H_3^{\text{ABA:eff}} = \gamma_1 \begin{bmatrix} 0 & z^* \\ z & 0 \end{bmatrix} \oplus \frac{\gamma_1}{\sqrt{2}} \begin{bmatrix} 0 & (-z^*)^2 \\ (-z)^2 & 0 \end{bmatrix} = H_1^{\text{eff}} \oplus H_2^{\text{eff}}/\sqrt{2}. \quad (101)$$

4.2.2. Landau levels Around the Dirac cones, we can expand the effective Hamiltonian, as in the monolayer case, as

$$H_1 \rightarrow H_1^{\text{eff}} = (\sigma \cdot X) \delta k_x + (\sigma \cdot Y) \delta k_y, \quad X = \begin{bmatrix} \text{Re} \Delta_x \\ -\text{Im} \Delta_x \\ 0 \end{bmatrix}, \quad Y = \begin{bmatrix} \text{Re} \Delta_y \\ -\text{Im} \Delta_y \\ 0 \end{bmatrix} \quad (102)$$

where $\Delta_\alpha = \frac{\partial \Delta}{\partial k_\alpha} \Big|_{k=K, K'}$. Then we have

$$(H_1^{\text{eff}})^2 = (\hbar c \overline{\delta k})^2, \quad \overline{\delta k}^2 \equiv [\delta k_x, \delta k_y] \Xi \begin{bmatrix} \delta k_x \\ \delta k_y \end{bmatrix}, \quad \Xi = \frac{1}{|X \times Y|} \begin{bmatrix} X \cdot X & Y \cdot X \\ X \cdot Y & Y \cdot Y \end{bmatrix} \quad (103)$$

where $c^2 = |X \times Y|/\hbar^2$ is an effective ‘‘light velocity’’ and $\overline{\delta k}$ is the averaged momentum near the Dirac cones with $\det \Xi = (|X|^2|Y|^2 - |X \cdot Y|^2)/|X \times Y|^2 = 1$. Note that

$$X \times Y = \begin{bmatrix} 0 \\ 0 \\ \text{Im} \Delta_x \Delta_y^* \end{bmatrix} = \begin{bmatrix} 0 \\ 0 \\ \chi \hbar^2 c^2 \end{bmatrix} \quad (104)$$

where $\chi = \text{sgn} \text{Im} \Delta_x \Delta_y^*$ is the chirality of the Dirac cones.

In a magnetic field, the Hamiltonian H_1^C in the continuum limit is obtained by replacing $\hbar \delta k_\alpha \rightarrow \pi_\alpha = p_\alpha - e A_\alpha = -i \hbar \partial_\alpha - e A_\alpha$ where $[\pi_x, \pi_y] = i \hbar e B = i(\hbar/\ell_B)^2$ with $\ell_B = \sqrt{\hbar/eB}$ ($eB > 0$). As for the ABC stacked p -layered graphene (including monolayer and bilayer), the effective continuum Hamiltonian is obtained as the extension of the McCann-Fal’ko [9] as

$$H_p^{\text{eff}} \rightarrow H_p^C \equiv (-\gamma_1)^{-(p-1)} \begin{bmatrix} 0 & (\Pi^\dagger)^p \\ \Pi^p & 0 \end{bmatrix}, \quad (105)$$

$$\Delta \rightarrow \Pi^\dagger \equiv \hbar^{-1} (\Delta_x \pi_x + \Delta_y \pi_y). \quad (106)$$

This is another derivation of the p -th layer effective Hamiltonian discussed by Koshino-McCann[10] for the chiral symmetric case. Here the commutation relation of Π is given as

$$[\Pi, \Pi^\dagger] = 2\hbar^{-2} \text{Im} \Delta_x \Delta_y^* = 2(c\hbar/\ell_B)^2 \chi. \quad (107)$$

Then one can define a canonical boson operator a , ($[a, a^\dagger] = 1$) as

$$\Pi = \begin{cases} a (c\hbar/\ell_B) \sqrt{2} & (\chi = +1) \\ a^\dagger (c\hbar/\ell_B) \sqrt{2} & (\chi = -1) \end{cases}. \quad (108)$$

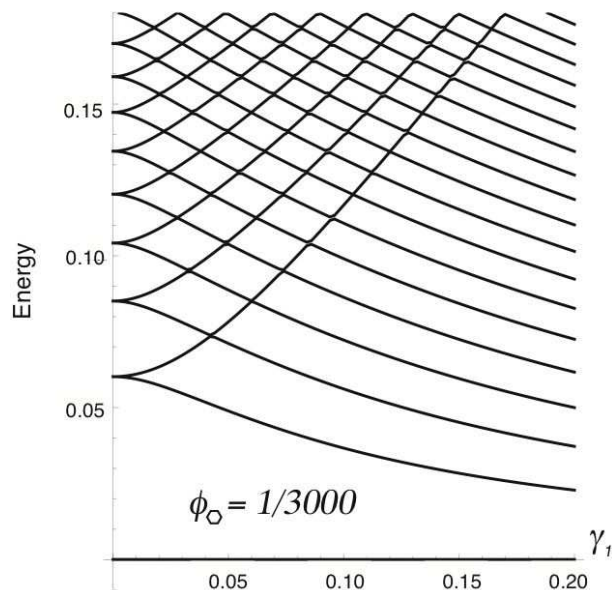


Figure 4. Low-energy Landau levels in the bilayer graphene for the magnetic field $\phi = 1/3000$ as a function of γ_1 (with $\gamma_0 = 1.0$ and $\gamma_3 = 0$ here).

For the positive chirality $\chi = +1$, one has

$$(H_p^C)^2 = N_p^2 \begin{bmatrix} (a^\dagger)^p a^p & 0 \\ 0 & a^p (a^\dagger)^p \end{bmatrix} = N_p^2 \begin{bmatrix} \prod_{i=1}^p (n - i + 1) & 0 \\ 0 & \prod_{i=1}^p (n + i) \end{bmatrix} \quad (109)$$

where $N_p = \gamma_1 (\gamma_1^{-1} c \sqrt{2e\hbar B})^p$, $n = a^\dagger a$, and

$$(a^\dagger)^2 a^2 = a^\dagger n a = (n - 1)n, \quad (a^\dagger)^3 a^3 = (n - 2)(n - 1)n, \quad \dots \quad (110)$$

$$a^2 (a^\dagger)^2 = (n + 2)(n + 1), \quad \dots \quad (111)$$

Then we have a series of non-equally spaced Landau levels as

$$E_n = \pm N_p \sqrt{n(n - 1)(n - 2) \cdots (n - p + 1)}. \quad (112)$$

The $\chi = -1$ case follows trivially.

4.3. Lifshitz transition in magnetic fields

In this section, let us focus on the Lifshitz transition caused by the trigonal warping term γ_3 , by calculating the energy levels on a honeycomb lattice. Using the chiral symmetry, we can diagonalize $D^\dagger D$ within the low-energy sector, which suffices to discuss the Landau levels near $E = 0$. Since D is a sparse matrix, we can handle quite small flux φ numerically using the lattice Hamiltonian.

Let us first show the energy levels of the bilayer graphene as a function of γ_1 in Fig.4. One can observe that larger γ_1 produces larger bonding-antibonding splitting, so that the low-energy sector is projected out from the high energy one.

Figure 5, on the other hand, displays the Landau levels as a function of the γ_3 . One can see that the Landau levels at $\gamma_3 = 0$ are adiabatically connected to two classes

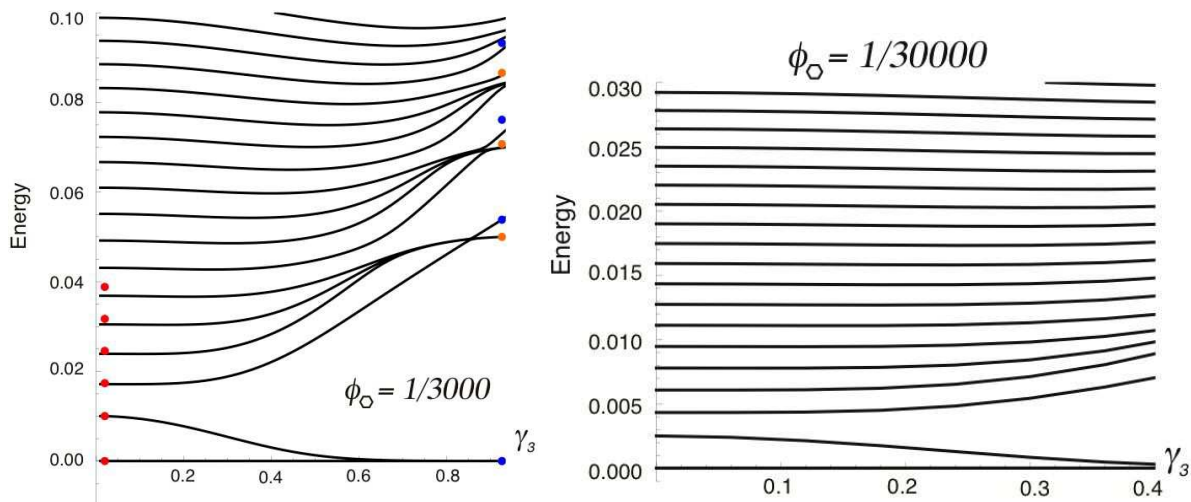


Figure 5. The Lifshitz transition caused by γ_3 is observed. (left) Low-energy Landau levels in the bilayer graphene in a magnetic field $\phi = 1/3000$ ($\gamma_0 = 1.0$ and $\gamma_1 = 0.5$). The red points at $\gamma_3 = 0$ denote a sequence $Const.\sqrt{n(n-1)}$, ($n = 0, 1, 2, \dots$). We have also displayed the sequences $\propto \sqrt{n}$ for $n = 0, 1, 2, 3$ (blue dots) and for $n = 1, 2, 3$ (orange). (right) The same plot for realistic $\gamma_1/\gamma_0 = 0.2$ and much smaller flux $\phi = 1/30000$.

of Landau levels at $\gamma_3 \neq 0$, which correspond to those of two kinds of 4 Dirac cones with different fermi velocity. To observe the phenomena at the moderate value of the flux, we take artificially large value for $\gamma_1/\gamma_0 = 0.5$ in the left pannel of the Figs.5. In the right pannel, the same plot for a much smaller, realistic γ_1 and the magnetic field.

5. Optical responses in bilayer and trilayer graphene

Let us move on to discuss optical responses in bilayer and trilayer graphene in the quantum Hall regime. We focus on the optical longitudinal conductivity $\sigma_{xx}(\omega)$, which descrones the optical absorption, and the optical Hall conductivity $\sigma_{xy}(\omega)$, which is directly related to the Faraday rotation, since the Faraday rotation angle Θ_H is proportional to $\sigma_{xy}(\omega)$ in the quantum Hall regime as

$$\Theta_H \simeq \frac{1}{(n_0 + n_s)c_0\varepsilon_0}\sigma_{xy}(\omega),$$

where c_0 is the speed of light and $n_0(n_s)$ is the refractive index of the air (substrate)[11].

The Faraday rotation for monolayer graphene is studied theoretically [12, 13], and experimentally starts to be measured [14]. Further, there are growing interests in the optical properties of bilayer and trilayer graphene, given that their electronic structures are distinct from that of monolayer graphene. As we have seen in Sec. 4, bilayer graphene has two parabolic bands touching at the K and K' points [15, 16]. Trilayer graphene comes with two different types of stacking, ABA and ABC, where the former

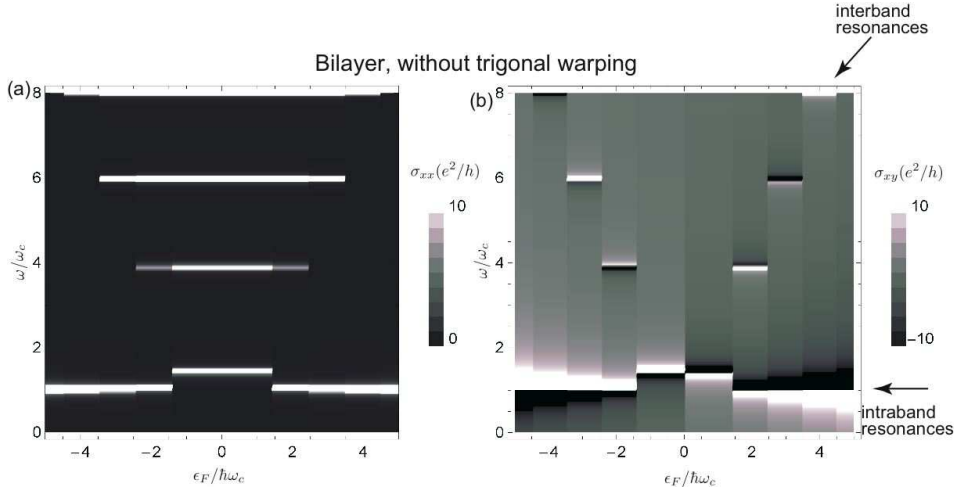


Figure 6. For the bilayer graphene QHE system without the trigonal warping effect ($\gamma_3 = 0$), we show (a) optical longitudinal conductivity $\sigma_{xx}(\epsilon_F, \omega)$, and (b) optical Hall conductivity $\sigma_{xy}(\epsilon_F, \omega)$ plotted against the Fermi energy ϵ_F and the frequency ω .

is described effectively as a mixture of monolayer and bilayer bands, while the latter shows a cubic band as Eq.105 with $p = 3$. Let us discuss optical responses for multilayer graphenes with these different lattice structures. Especially, we argue the effect of the presence or absence of the chiral symmetry gives a significantly different optical responses of $n = 0$ LL in ABA trilayer graphene.

The optical longitudinal ($\sigma_{xx}(\omega)$) and Hall ($\sigma_{xy}(\omega)$) conductivities are evaluated from the Kubo formula as

$$\sigma_{\alpha\beta}(\omega) = \frac{\hbar}{iL^2} \sum_{ab} j_{\alpha}^{ab} j_{\beta}^{ba} \frac{f(\epsilon_b) - f(\epsilon_a)}{\epsilon_b - \epsilon_a} \frac{1}{\epsilon_b - \epsilon_a - \hbar\omega - i\eta}, \quad (113)$$

where $f(\epsilon)$ is the Fermi distribution, ϵ_a eigenenergies, η a small energy cutoff for a stability of the calculation, and j_{α}^{ab} is the matrix element of the current operator $j = \partial H / \partial A$.

5.1. Bilayer graphene

We start with calculating the optical Hall conductivity using Kubo formula Eqn.113 for the bilayer system without the trigonal warping effect (Eq.105 with $p = 2$). The result for the optical longitudinal and Hall conductivities are shown in Fig.6(a,b). If we label LLs with the Landau index n and an electron/hole band index $s = \pm$, an intra-band transition $(n, s) \rightarrow (n + 1, s)$ occurs around

$$\omega_{\text{intra}} \sim \omega_{\text{bilayer}} = 2v^2eB/\gamma_1,$$

with the Fermi velocity of the Dirac cone v ($= c$ in Sec. 4), since LLs are almost equally spaced, unlike in the monolayer case where LL energy $\propto \sqrt{n}$ is not equally separated.

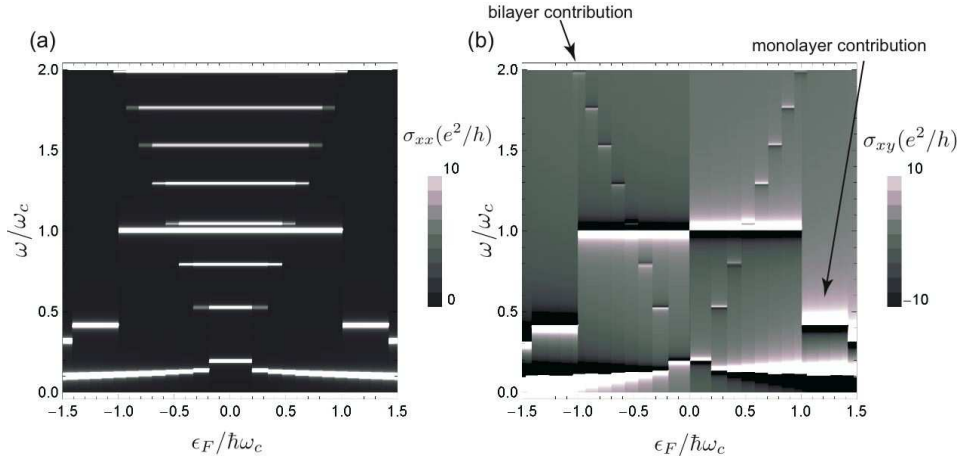


Figure 7. For the ABA-stacked trilayer graphene QHE system (with $\gamma_1/\hbar\omega_c = 5$) we show (a) optical longitudinal conductivity $\sigma_{xx}(\epsilon_F, \omega)$, and (b) optical Hall conductivity $\sigma_{xy}(\epsilon_F, \omega)$ plotted against the Fermi energy ϵ_F and frequency ω .

On top of this, there are inter-band transitions across the band-touching point, obeying a selection rule $(n, -s) \rightarrow (n + 1, s)$. Thus the inter-band transition occurs around

$$\hbar\omega_{\text{inter}} \simeq 2|\epsilon_F|,$$

for large enough n .

5.2. ABA trilayer graphene

For ABA stacked trilayer, the effective Hamiltonian around K_+/K_- points is given by a 6×6 matrix (the dimension being 2 sublattices \times 3 layers) as [17, 18, 19, 20]

$$H_{\text{ABA}} = \begin{pmatrix} 0 & v\pi^\dagger & 0 & v_3\pi & \gamma_2/2 & 0 \\ v\pi & \Delta' & \gamma_1 & 0 & 0 & \gamma_5/2 \\ 0 & \gamma_1 & \Delta' & v\pi^\dagger & 0 & \gamma_1 \\ v_3\pi^\dagger & 0 & v\pi & 0 & v_3\pi^\dagger & 0 \\ \gamma_2/2 & 0 & 0 & v_3\pi & 0 & v\pi^\dagger \\ 0 & \gamma_5/2 & \gamma_1 & 0 & v\pi & \Delta' \end{pmatrix}, \quad (114)$$

with $\pi = \pi_x + i\pi_y$, a velocity v_3 associated with γ_3 as $v_3 = v\gamma_3/\gamma_0$, Δ' the on-site energy difference between the atoms with and without vertical bond γ_1 , and $\gamma_2(\gamma_5)$ the next-nearest interlayer hoppings between $A1$ and $A3$ ($B1$ and $B3$).

First, we only retain γ_0, γ_1 terms in Eq.114, in which case the Hamiltonian is chiral-symmetric. In Fig.7(a,b), the optical longitudinal and Hall conductivities $\sigma_{xx}(\epsilon_F, \omega), \sigma_{xy}(\epsilon_F, \omega)$ are plotted against the Fermi energy ϵ_F and frequency ω . The magnetic field is chosen so that an interlayer hopping energy is $\gamma_1/\hbar\omega_c = 5$, with the monolayer cyclotron energy $\omega_c = \sqrt{2}v/\ell = v\sqrt{2eB/\hbar}$. We can see a monolayer contribution (Dirac cyclotron frequency = ω_c) and a bilayer contribution with a cyclotron energy, $\hbar\omega_{\text{bilayer}}/\sqrt{2}$, both of which show intra-band and inter-band transitions.

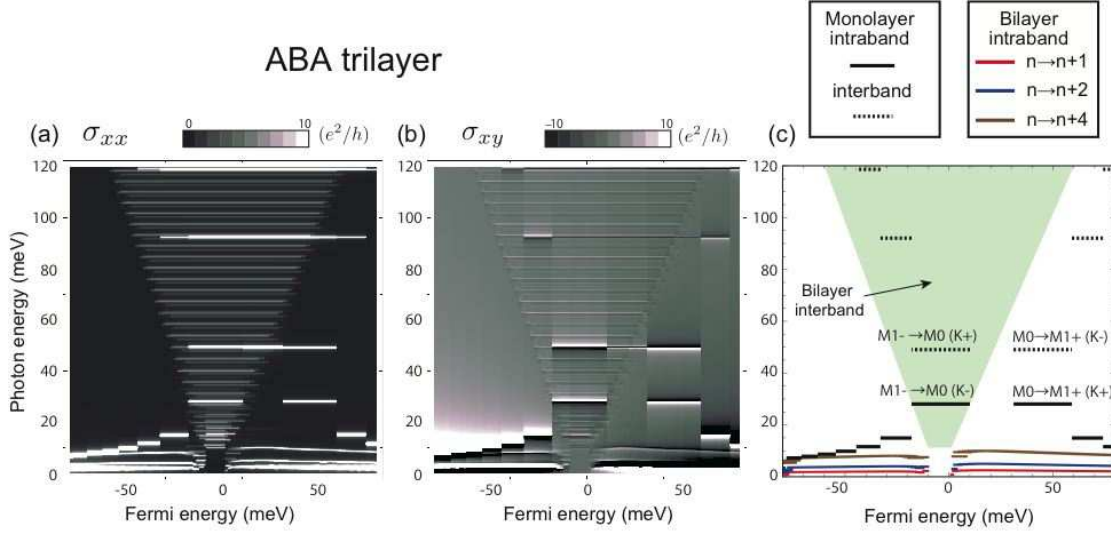


Figure 8. (a) Longitudinal $\sigma_{xx}(\epsilon_F, \omega)$ and (b) Hall $\sigma_{xy}(\epsilon_F, \omega)$ plotted against the Fermi energy ϵ_F and the frequency ω for a magnetic field $B = 1T$. (c) A diagram indicating allowed resonances in σ_{xy} .

For moderate magnetic fields $B \sim 1$ T, cyclotron frequency for monolayer is much larger than that for bilayer $\omega_c \gg \omega_{\text{bilayer}}$. In this case, σ_{xx} is an even function with respect to $\epsilon_F = 0$, while σ_{xy} is odd due to the electron-hole symmetry, a consequence of the chiral symmetry. The jump of σ_{xy} at $\epsilon_F = 0$ is related to the chiral zero modes.

Now, if we include all the hopping terms in Eq.114, the chiral symmetry is broken, and we no longer have the chiral protection for zero modes (three zero energy LLs). We have then a massive Dirac band plus gapped bilayer bands with energy shifts. As for hopping parameters, we adopt the values for graphite, $\gamma_0 = 3.2$ eV, $\gamma_1 = 0.39$ eV, $\gamma_3 = 0.32$ eV, $\gamma_2 = -0.020$ eV, $\gamma_5 = 0.038$ eV, $\Delta' = 0.050$ eV [21, 7]. Figures 7(a,b) depict the result for the optical longitudinal $\sigma_{xx}(\epsilon_F, \omega)$ and Hall conductivity $\sigma_{xy}(\epsilon_F, \omega)$ plotted against the Fermi energy ϵ_F and frequency ω for ABA stacked trilayer graphene QHE system. We see contributions from monolayer-like Dirac LLs (labeled with M) and those from bilayer LLs (B), both of which exhibit intra-band and inter-band transitions. Since Dirac cone is massive due to the chiral symmetry breaking and the zero-energy LL for the monolayer band (M0) is situated at the bottom of the conduction band for K_+ valley and the top of the valence band for K_- , $M0 \rightarrow M(1, +)$ resonance occurs at an energy lower than $M(1, -) \rightarrow M0$ for K_+ , and vice versa for K_- . A cancellation of resonances in σ_{xy} , due to the opposite signs in current matrices, occurs between $M(1, -) \rightarrow M0$ for K_+ and $M0 \rightarrow M(1, +)$ for K_- for a region of Fermi energy between $M0(K_+)$ and $M0(K_-)$, while this is not the case with σ_{xx} . For bilayer contributions, satellites appear as $B(n, \pm) \leftrightarrow B(n + 1 + 3m, \pm)$ and $B(n, \pm) \leftrightarrow B(n + 2 + 3m, \pm)$, since the trigonal warping term mixes n LLs and $n + 3$ LLs [22]. The resonance frequency for intra-band transition within the conduction band is larger than those within the valence band, which is a consequence of the electron-hole asymmetry in the bilayer bands, triggered

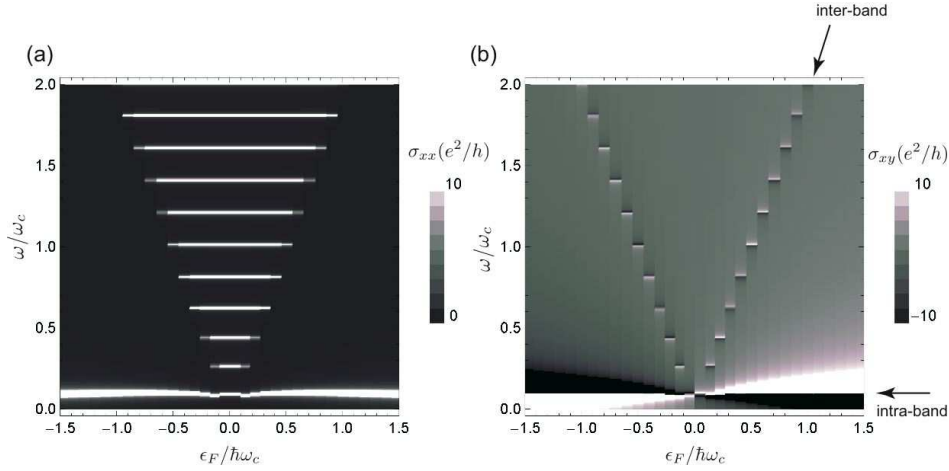


Figure 9. For ABC-stacked trilayer graphene QHE system (with $\gamma_1/\hbar\omega_c = 5$) we show (a) optical longitudinal conductivity $\sigma_{xx}(\epsilon_F, \omega)$, and (b) optical Hall conductivity $\sigma_{xy}(\epsilon_F, \omega)$ plotted against the Fermi energy ϵ_F and frequency ω .

by a breaking of the chiral symmetry. A deviation in the cyclotron mass for electron and hole bands prevents a complete cancellation between $B(n, -) \rightarrow B(n+1, +)$ and $B(n+1, -) \rightarrow B(n, +)$ transitions, which results in small interband transitions in a wide region of Fermi energy.

5.3. ABC trilayer graphene

The low energy effective Hamiltonian of ABC stacked trilayer graphene in a 2 by 2 matrix Eq.105 is a cubic form in the momentum, if we neglect hopping terms but γ_0, γ_1 . For this effective Hamiltonian, LL energy (Eq.112) shows a magnetic-field dependence $\propto B^{\frac{3}{2}}$, resulting in a smaller LL spacing compared to the single-layer $\text{LL} \propto B^{\frac{1}{2}}$ and bilayer $\text{LL} \propto B$ for weak magnetic fields.

Now we turn to a result for the optical conductivities in ABC trilayer for an interlayer hopping energy $\gamma_1/\hbar\omega_c = 5$, with monolayer cyclotron frequency $\omega_c = v\sqrt{2eB/\hbar}$. Figures 9(a,b) show the optical longitudinal and Hall conductivity $\sigma_{xy}(\epsilon_F, \omega)$ plotted against the Fermi energy ϵ_F and frequency ω for ABC stacked trilayer graphene QHE system. In contrast to ABA stacking (Fig.7), we only see a single sequence of intra-band and inter-band transitions with a much smaller cyclotron energy than $\hbar\omega_c$ due to the dependence on magnetic fields $\propto B^{\frac{3}{2}}$. The inter-band transition occurs at $\hbar\omega \sim 2\epsilon_F$ for the same reason as in the bilayer, while the intra-band transition energy grows with increasing LL index n as

$$\omega \sim (n+1)^{3/2} - n^{3/2} \sim n^{\frac{1}{2}},$$

which explains why the intra-band resonance energy increases with n in Fig.9(d), while it decreases with n in the case of the monolayer graphene [13]. We can then predict in general that, for ABC p -layered graphene, the intra-band transition occurs

at $\omega \sim n^{p/2-1}$, and the inter-band transition at $\omega \sim 2\epsilon_F$. Thus we end up with the intra-band transition energies that exhibit different behaviors with Landau index n for monolayer ($\propto n^{-1/2}$), bilayer (constant) and ABC trilayer ($\propto n^{1/2}$) graphenes, while the inter-band transition energies are qualitatively the same with $\sim 2\epsilon_F$.

Acknowledgement

We thank Mikito Koshino for fruitful discussions. The work is supported in part by Grants-in-Aid for Scientific Research, No.23340112 and No.23654128 from JSPS. The computation in this work has been done in part with the facilities of the Supercomputer Center, Institute for Solid State Physics, University of Tokyo.

References

- [1] Novoselov K S, Geim A K, Morozov S V, Jiang D, Katsnelson M I, Grigorieva I V, Dubonos S V and Firsov A A 2005 *Nature* **438** 197
- [2] Zhang Y, Tan Y, Stormer H and Kim P 2005 *Nature* **438** 201
- [3] Sadowski M L, Martinez G, Potemski M, Berger C and de Heer W A 2006 *Phys. Rev. Lett.* **97**(26) 266405
- [4] Berry M V 1984 *Proc. R. Soc.* **A392** 45
- [5] Nielsen H B and Ninomiya M 1981 *Nucl. Phys. B* **185** 20
- [6] Hatsugai Y, Fukui T and Aoki H 2006 *Phys. Rev. B* **74** 205414
- [7] Dresselhaus M and Dresselhaus G 2002 *Advances in Physics* **51** 1–186
- [8] Dresselhaus M and Dresselhaus G 1981 *Advances in Physics* **30** 139–326
- [9] McCann E and Fal'ko V I 2006 *Phys. Rev. Lett.* **96**(8) 086805
- [10] Koshino M and McCann E 2009 *Phys. Rev. B* **80**(16) 165409 URL <http://link.aps.org/doi/10.1103/PhysRevB.80.165409>
- [11] O'Connell R F and Wallace G 1982 *Phys. Rev. B* **26** 2231–2234
- [12] Gusynin V P, Sharapov S G and Carbotte J P 2007 *J. Phys.: Condens. Matter* **19** 026222
- [13] Morimoto T, Hatsugai Y and Aoki H 2009 *Phys. Rev. Lett.* **103** 116803
- [14] Crassee I, Levallois J, Walter A, Ostler M, Bostwick A, Rotenberg E, Seyller T, Van Der Marel D and Kuzmenko A 2010 *Nature Physics*
- [15] Novoselov K, McCann E, Morozov S, Fal'ko V, Katsnelson M, Zeitler U, Jiang D, Schedin F and Geim A 2006 *Nature Physics*. **2** 177–180
- [16] McCann E and Fal'ko V 2006 *Phys. Rev. Lett.* **96** 86805
- [17] Guinea F, Castro Neto A H and Peres N M R 2006 *Phys. Rev. B* **73**(24) 245426
- [18] Partoens B and Peeters F 2006 *Physical Review B* **74** 075404
- [19] Lu C, Chang C, Huang Y, Chen R and Lin M 2006 *Physical Review B* **73** 144427
- [20] Koshino M and Ando T 2007 *Phys. Rev. B* **76**(8) 085425
- [21] Charlier J, Gonze X and Michenaud J 1991 *Phys. Rev. B* **43** 4579
- [22] Abergel D S L and Fal'ko V I 2007 *Phys. Rev. B* **75**(15) 155430